Fiber Optic Pressure Sensor Using a Conformal Polymer on Multimode Interference Device

Daniel A. May-Arrioja, Victor I. Ruiz-Perez, Yaneth Bustos-Terrones, and Miguel A. Basurto-Pensado

***Abstract*— We report experimental results on an optical fiber pressure sensor based on multimode interference effects (MMIs). The key component is a small multimode fiber (MMF) section without cladding, which is placed on a direct contact with a polydimethilsiloxane polymer layer previously attached to a pressure-sensitive membrane. When the applied pressure is increased, both the polymer contact area and the induced stress on the MMF increase directly proportional with the applied pressure. Both effects contribute to losses of the propagating modes, and since the MMI spectrum is formed by the interference of the propagating modes, the net effect is that the intensity of the spectral response of the MMI is reduced as the pressure is increased. Therefore, by tracking a single wavelength, the intensity changes are correlated to the applied pressure values. The response of the sensor is highly linear within a pressure range of 0–960 kPa with a sensitivity of -0.145×10^{-3} mW/kPa. The key features of the MMI pressure sensor are its low-cost and high repeatability.**

***Index Terms*— Pressure, multimode interference, fiber sensor.**

I. Introduction

PRESSURE measurements are a strategic technology in many industrial applications. Due to its importance, modern technology tools are taken into account in the development of pressure sensors which are able to reliably operate in harsh environments. Pressure sensors based on optical fiber technology have gained rapid acceptance, due to its dielectric nature, passivity, flexibility, and small size, among others advantages. These attractive characteristics make them ideal to operate under extreme environmental conditions such as strong electromagnetic interference, exposure to toxic and corrosive elements, difficult access, and high pressure and temperature.

Over the years different schemes based on optical fibers have been employed as pressure sensors. According to their principle operation, we can classify them as spectral and intensity based sensors. Spectral based sensors typically operate by tracking the wavelength shift of a peak/valley as the applied pressure is changed. Fiber Bragg gratings (FBG) have been widely investigated as pressure sensors under different configurations [1]–[3]. For instance, pressure can be laterally applied to compress the FBG in order to induce birefringence, which splits the resonance peak in two peaks and by measuring their peak separation the applied pressure can be measured [1]. Assembling an adequate transducing mechanism allows to effectively apply either compressive or tensile strain to the FBG, as well as bending of the FBG. Therefore, pressure is detected by following the peak spectral shift of the FBG resonance [2], [3]. Regardless of the technique, the highest sensitivity achieved with FBG is on the order of 3.5 pm/kPa. As a natural extension of the technique, long period gratings (LPG) have been also used as pressure sensors [4], [5] using similar schemes as with FBG, and a maximum sensitivity of 0.06 pm/kPa can be obtained with such structures. In the case of micro-structured fibers and photonic crystal fibers (PCF), the holey structure along the fiber provides a flexible fiber structure that can be compressed more easily when inserted in a pressure chamber. Such distortions are correlated with spectral changes on the fiber response, which enable us to measure the pressure in the chamber [6]–[8]. This approach provides sensitivities on the order of 3.42 nm/MPa and resolution on the order of 2.9 kPa [8], but they require expensive specialty fibers. A different approach relies on the fabrication of membranes or diaphragms on the tip of a single-mode fiber (SMF) in order to form a Fabry-Perot cavity [9], [10]. When pressure is applied to the fiber tip this will change the cavity length, which can be extracted from the interference fringes. Using a membrane with an optimum thickness provides sensitivities as high as 70.5 nm/kPa [10] and resolution of 0.3 kPa [9]. The main disadvantages of spectral sensors are related to the need of fibers with special structures, expensive fibers, and complex fabrication processes. In addition, in order to read such sensors an optical spectrum analyzer (OSA) is required which impacts the final cost of a sensor for commercial applications. Intensity based sensors, on the other hand, have the advantage that they are fabricated using simple fibers and they do not require an OSA. The simplest setup consists of a multimode fiber (MMF) which is perpendicularly aligned to a mirror, and the reflected light is coupled back to the MMF. The mirror moves away from the MMF when pressure is applied and the intensity is then reduced [11]. The fiber can be also bended as a function of pressure, applying either micro or macro bending, and this

Manuscript received February 15, 2015; revised November 24, 2015; accepted December 2, 2015. Date of publication December 18, 2015; date of current version February 10, 2016. This work was supported by the Consejo Nacional de Ciencia y Tecnología under Grant CB-2008/101378 and Grant CB-2010/157866. The work of V. I. Ruiz Perez was supported by the Consejo Nacional de Ciencia y Tecnología through a Post-Doctoral Scholarship. The associate editor coordinating the review of this paper and approving it for publication was Dr. William N. MacPherson.

D. A. May-Arrioja is with the Fiber and Integrated Optics Laboratory, Centro de Investigaciones en Optica, Aguascalientes 20200, Mexico (e-mail: darrioja@cio.mx).

V. I. Ruiz-Perez and Y. Bustos-Terrones are with the Departamento de Ingenieria Ambiental, Insituto Tecnologico de Culiacan, Culiacán 80220, México (e-mail: victoryvan1@hotmail.com; yanethbt@hotmail.com).

M. A. Basurto-Pensado is with the Center for Research in Engineering and Applied Science, Universidad Autónoma del Estado de Morelos, Cuernavaca 62209, Mexico (e-mail: mbasurto@uaem.mx).

Digital Object Identifier 10.1109/JSEN.2015.2510360

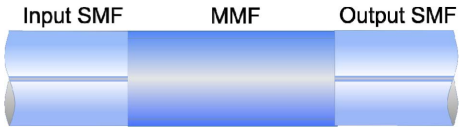

Fig. 1. Schematic of the multimode interference fiber device.

also provides intensity changes as a function of the applied pressure. Such sensors provide sensitivities on the order of 2.5×10^{-3} mW/kPa [12].

In this work, we propose and demonstrate a simple alternative to develop a pressure sensor by incorporating a multimode interference (MMI) fiber structure. The operation of the sensor relies on a conformal elastomer whose contact area around the circumference of the MMF increases as a function of applied pressure. Since we use a MMF known as No-Core fiber (NCF), which is basically a MMF without cladding (the clad is air), the polymer modifies the cladding of the NCF. In addition, the applied pressure on the NCF induces mechanical stress which modifies the RI distribution of the NCF core. The net effect of both contributions is to effectively reduce the intensity of the transmitted MMI spectrum. Intensity changes are obtained by tracking a particular wavelength, which are directly correlated to the pressure values. Using this configuration a linear response and high repeatability are easily obtained.

II. Sensing Principle

The basis for the proposed sensor relies on a MMI device and is schematically shown in Fig. 1. The MMI structure, also known as SMS structure [13], consists of a small section of MMF spliced between two SMF.

The operational principle behind a MMI structure can be summarized as follow. When the fundamental mode reaches the MMF section, it excites the guided modes that can be supported by the MMF. As the modes propagate along the MMF, the interference between the modes will give rise to the formation of self-images of the input field. This particular effect occurs at selected locations and is related to the accumulated phase. In this respect, given that each mode has a particular field profile, they will experience a different phase change as they travel similar distances. Nevertheless, there will be certain position where the accumulated phase difference between any two excited modes will be very close to or a multiple of 2π. When this occurs, we have constructive interference between the guided modes, which gives rise to the reproduction of the input field profile at certain positions inside the MMF. The length L where these self-images occur can be estimated by [14],

$$L = p\frac{4n_{MMF}D_{MMF}^2}{\lambda_0} \quad with \;\; p = 0, 1, 2, \ldots \tag{1}$$

where λ_0 is the wavelength in free-space, n_{MMF} and D_{MMF} are the effective RI and the core diameter of the fundamental mode of the MMF, respectively. The p factor denotes the periodicity of the self-imaging process along the MMF. As shown in Eq. (1), once we know the MMF parameters, we can easily determine the required MMF length that will form a self-image of the input field at the end facet of this MMF segment for a specific light wavelength. This corresponds to points of maximum coupling from the input SMF to the output SMF. It is important to notice that if light with a wavelength that is different from the design value is used, the corresponding self-image will be formed either before or after the end facet of the MMF. As a result, the coupled intensity will be lower for those detuned wavelengths. Therefore, when a broadband source is launched through the MMI device, we obtain a band-pass filter response. Such response can be used for sensing applications if the MMI structure is properly designed.

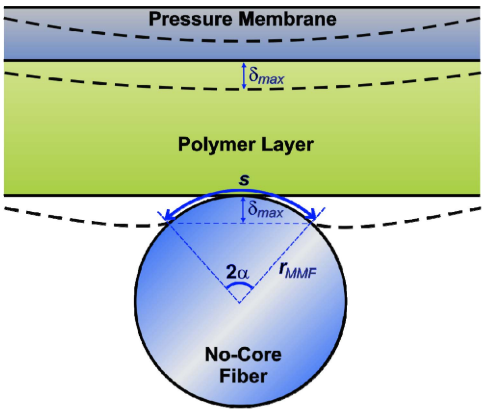

Fig. 2. Geometry of contact area between PDMS layer and NCF.

The key concept in order to employ the proposed structure as a pressure sensor relies on the fact that, when the RI of the core, cladding, or both is modified, the number of modes supported by the MMF fiber is also modified. Since the MMI signal is formed by the constructive interference of the propagating modes, such changes on the number of propagating modes modify the intensity of the transmitted MMI signal. In order to use this effect as a pressure sensor, a thin polymer layer is attached to a pressure membrane that is bended under applied pressure as shown by the transversal view of Fig. 2. The optical fiber used in the sensor is a MMF known as No-Core fiber (NCF), which is basically a MMF without cladding, i.e. the clad is air. The NCF is initially placed in minimal contact with the polymer layer, as shown by the solid tangent line of the polymer on the NCF in Fig. 2. When the membrane is bended under applied pressure the polymer will gradually conform to the NCF surface and the contact area is increased as the pressure is raised, which is also shown by the dashed line in Fig. 2. Since the NCF does not have a cladding, the polymer film covering the NCF acts as an asymmetric cladding. Additionally the polymer film is compressing the NCF and this induces RI changes in the core of the NCF due to stress-optic effects of the silica. The net effect is to reduce the RI contrast between the NCF core and the asymmetric polymer cladding, which effectively reduce the number of propagating modes. Therefore, we should observe a reduction of the transmitted MMI signal as the pressure is increased. We should emphasize that this is feasible as long as the RI of the polymer is lower than that of the

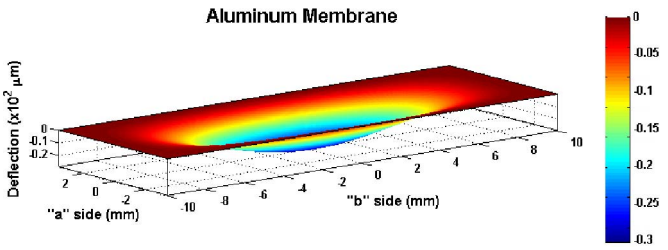

Fig. 3. Deflection of a rectangular aluminum membrane.

NCF in order to maintain waveguiding conditions. The polymer used in our experiments was Polydimethilsiloxane (PDMS) made by Dow Corning (Sylgard Elastometer 184). The RI of PDMS is 1.4194 at 1550 nm with negligible absorption at this wavelength [15]. The advantage of PDMS is that after curing is a relatively soft material (Young's modulus of ~0.75 MPa) [16]. Therefore, when the PDMS is pressed on an object with shallow variations it will follow the shape of the object.

Since the RI change of core and cladding are directly related to the contact area, it is important to obtain the response of the contact area as a function of the applied pressure. Considering the dimensions of the NCF, we choose a membrane with a rectangular geometry. The deflection δ of a rectangular membrane with sides $2a$ and $2b$ and thickness h, peripherally clamped and subjected to a normal pressure P, can be calculated by the approximated expression for small deflection ($\delta < 0.3$h) [17],

$$\delta(x,y) = \frac{4Pa^4b^4}{\pi^4 D\left(3a^4+3b^4+2a^2b^2\right)} \times \left(1+\cos\frac{\pi x}{a}\right)\left(1+\cos\frac{\pi y}{b}\right), \quad (2)$$

where D is the flexural rigidity of the membrane defined as $D = Eh^3/12(1-\nu^2)$, with E as the Young's modulus and ν as the Poisson's ratio. We selected aluminum as the membrane material because is quite simple to manufacture while being a highly robust packaging material. In the case of aluminum we have an E value of 69 MPa and ν of 0.34. Using Eq. (2) we can plot the deflection δ of an aluminum membrane for a given pressure. For instance, the deflection of an aluminum membrane with dimensions of 7 mm × 20 mm and thickness $h = 0.3$ mm, at a pressure of 700 kPa is shown in Fig. 3. We should highlight that by changing the membrane thickness we can control the maximum deflection for a given maximum pressure. The membrane thickness in Fig. 3 corresponds to the optimum displacement in our setup at a maximum pressure of 1200 kPa.

By inspection of the geometry in Fig. 2 we can observe that as the PDMS is moved against the fiber, only a portion of the PDMS defined by the arc length $s = 2r_{MMF}\alpha$ makes contact with the NCF. Since the contact area A is simply $A = sL$, it can be finally expressed as a function of δ_{max} by,

$$A = 2Lr_{MMF}\cos^{-1}\left(1-\frac{\delta_{\max}}{r_{MMF}}\right), \quad (3)$$

where δ_{max} is obtained from Eq. (2) by setting x = y = 0.

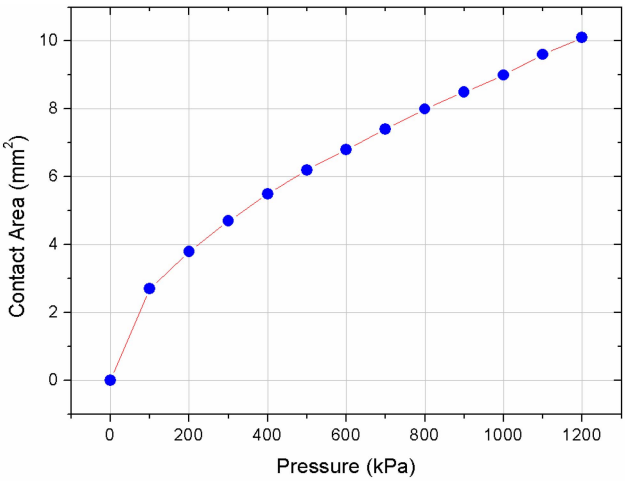

Fig. 4. Contact area as a function of applied pressure.

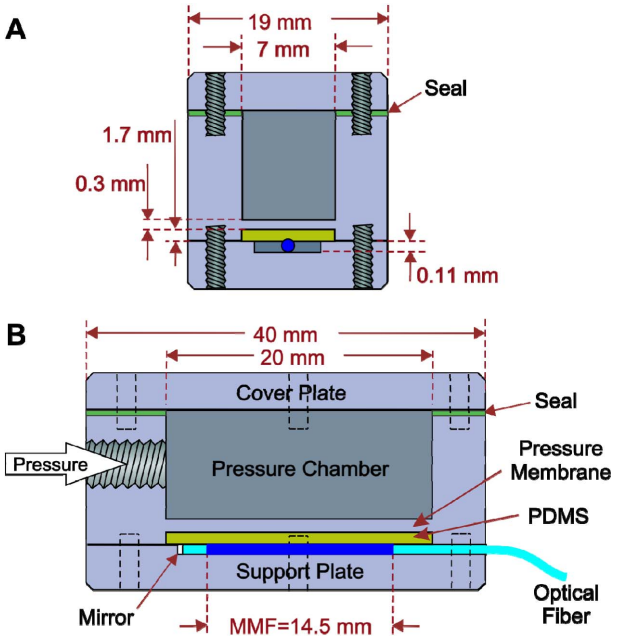

Fig. 5. Schematic of the assembled pressure sensor. a) Transversal cross section. b) Longitudinal cross section.

Using Eq. (2) and (3) we can then estimate the effective contact area as a function of the applied pressure. As shown in Fig. 4 the contact area increases very rapidly for low pressures and slowly, but quite linear, after a particular pressure value. Therefore, we can expect that the intensity changes of the transmitted MMI signal should also follow a similar profile. Although the response is not linear when we start applying pressure, we can design our sensor in such a way that an initial pressure is applied to the NCF in order to obtain a linear response across the entire sensing range.

III. Experimental Setup

A schematic of the pressure sensor using the MMI device is shown in Fig. 5. The main components are a small pressure chamber and a support plate in which the SMS structure

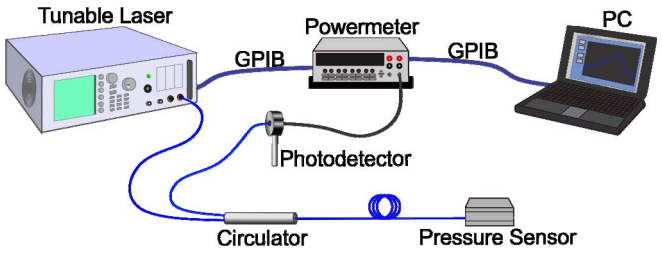

Fig. 6. Experimental setup for characterization of the MMI pressure sensor.

is placed. The pressure chamber was built by machining a rectangular cavity through an aluminum block with dimensions of 4.0 cm × 1.9 cm × 1.2 cm. The depth of the cavity was 1.0 cm with sides of 0.7 cm × 2.0 cm. Similarly, over the opposite side, we machined a cavity with same lateral dimensions but a smaller cavity depth of 1.7 mm leaving a thin aluminum membrane with a thickness of 0.3 mm. The chamber was hermetically sealed using an aluminum cover plate held by screws. An inlet for the applied pressure was drilled on one sidewall of the chamber. The liquid PDMS is poured directly in the cavity of the pressure chamber and the excess polymer is removed using a flat blade leaving PDMS only in the cavity. In this way we obtain a consistent PDMS layer with a thickness of 1.7 mm. The PDMS was cured by placing the support plate in a hotplate at 60 °C for 2 hrs. The SMS structure was attached to an aluminum support in which we machined another rectangular cavity with lateral dimensions of 0.5 cm × 2.6 cm. We fabricated a support plate with a depth of 125 μm that allows the NCF to make soft contact with the PDMS layer. We also fabricated another support plate with a depth of 110 μm that allows us to have an initial contact between the polymer layer and the NCF as was suggested before in order to linearize the sensor response. The SMS was centered at the support plate cavity and attached with a thin layer of epoxy. The output SMF had a length of 2 mm with a gold mirror deposited at its end facet. The mirror was fabricated by inserting the output SMF in a silica ferrule (127 μm inner diameter) until it reaches the other end of the ferrule. The ferrule provides protection of the un-cladded NCF. The fiber is fixed to the ferrule using a drop of photoresist, and the whole assembly is placed in a thermal evaporator. A 3 nm chromium layer is evaporated to act as an adhesion layer followed by 200 nm of gold to form the mirror. The pressure chamber was finally connected to a nitrogen cylinder and the input pressure was controlled with a needle valve and monitored by a digital pressure gauge (Crystal Engineering M1-3KPSI).

IV. Experimental Results

The sensor was evaluated using the experimental setup shown in Fig. 6. A tunable laser (Hewlett Packard 8164A) with a wavelength range from 1450 to 1620 nm was connected via a circulator to the pressure sensor and the light reflected back for each wavelength was monitored with a photodetector (Newport 818-IG-L-FC/DB) and a powermeter (Newport 1830-R).

The MMI device was fabricated by first splicing a section of SMF to the NCF. After this, the NCF is exactly measured

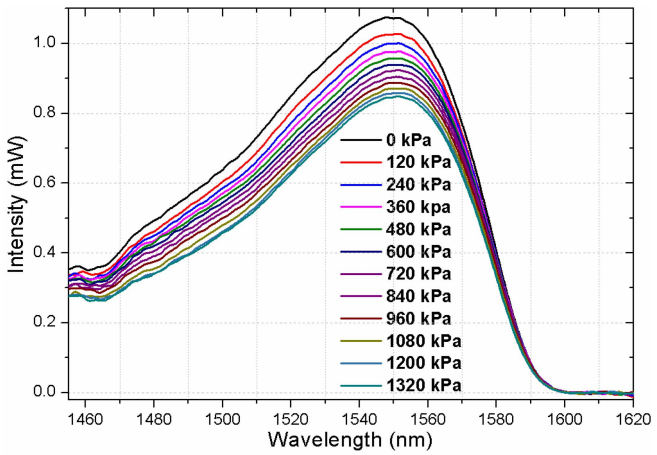

Fig. 7. Spectral response of MMI pressure sensor.

using a micrometer stage and cleaved to the right length, and this facet is spliced to another SMF. This second SMF is cleaved at a length of 2 mm and the facet is coated with 200 nm of gold that acts as a mirror. The length of the No-Core fiber was 14.55 mm, which corresponds to a MMI peak wavelength of 1550 nm. We should mention that even when lower insertion losses in MMI devices are obtained for the fourth self-image [18], we have chosen the first self-image in order to obtain a more compact sensor design. This is not a detrimental effect in our application, as will be shown later, and also provides a greater tolerance to errors in the accuracy of the MMF length [13]. After the MMI device is attached to the support plate and the sensor is assembled as described in the last section, the measurements are acquired as follow. Pressure is applied to the pressure chamber with increments of approximately 120 kPa, and at each pressure value the tunable laser is scanned in steps of 0.1 nm and the light reflected back from the sensor is measured at each wavelength using the photodetector and powermeter. This provides a full picture of the transmitted spectrum as a function of the applied pressure. Measurements were taken using the support plate with a depth of 125 μm, and the results are shown in Fig. 7. These measurements correspond to a pressure range from 0 to 1320 kPa. We can observe that as the pressure is increased the MMI spectral response is attenuated, which is correlated with the loss of high order modes as the PDMS is making contact with the NCF.

By plotting the peak MMI wavelength (1550 nm) as a function of the applied pressure we can observe in detail the response of the sensor (Fig. 8). We can observe that for low pressures below 120 kPa the intensity is reduced very rapidly, and for pressures beyond 120 kPa the intensity decreases monotonically as the pressure is increased. We should highlight that the sensor response is quite similar as compared to that of Fig. 4. This reveals that in fact the perturbation of the transmitted intensity is directly related with the contact area between the PDMS polymer and the NCF. As shown in Fig. 8, by having an initial pressure between the PDMS layer and the NCF we can shift the starting point of the sensor in order to obtain a linear response over the entire sensing range. This was achieved by reducing the initial depth of 125 μm of

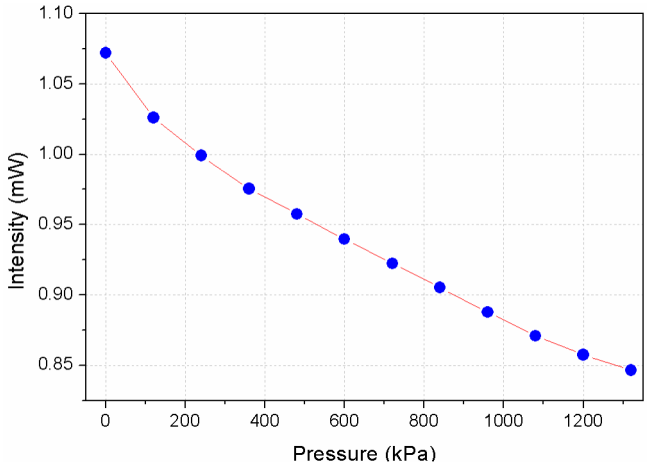

Fig. 8. Intensity vs Pressure at wavelength of 1550 nm.

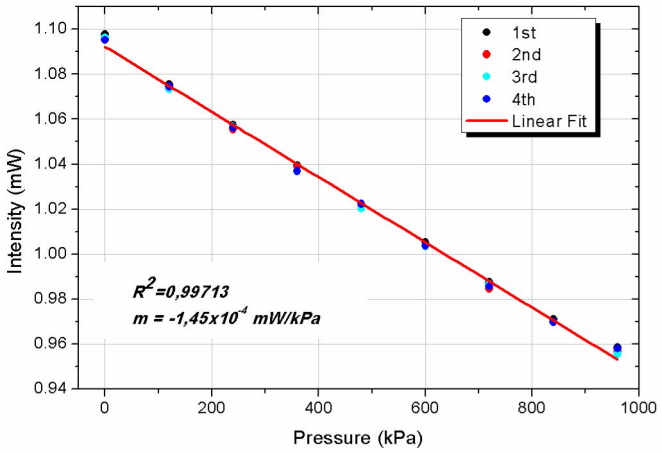

Fig. 9. Transmitted intensity at the linear range ($\lambda = 1550$ nm).

the cavity in the support plate. We fabricated several support plates in which the cavity depth was reduced in steps of 5 μm, and each support plate is used to evaluate the linearity of the sensor response. After this optimization process for the initial contact, we found an excellent linear response using a support plate with a cavity depth of 110 μm. The sensor response can be observed in Fig. 9 by plotting the MMI peak intensity as a function of the applied pressure. A good correlation coefficient R^2 with a value of 0.99713 can be estimated. The only drawback of this linearization scheme is that the sensing range is reduced from 0 kPa to 960 kPa. Nevertheless, the pressure range can be increased if the thickness of the pressure membrane is increased.

The repeatability of the sensor was characterized by performing four consecutive measurements from 0 to 960 kPa. As shown in Fig. 9, we can observe that the sensor response is highly reproducible at each measurement, and a sensitivity of -0.145×10^{-3} mW/kPa can be calculated by applying a linear fitting. We should also highlight that although initially we need to characterize the spectral response of the sensor, after the operating wavelength is selected we can use a single wavelength diode laser instead of the tunable laser. This was the case for the measurements shown in Fig. 9 were the data was acquired by measuring the transmitted intensity at the wavelength of interest. Based on the dispersion data of Fig. 9 we can estimate a resolution of 5 kPa. The resolution could be enhanced by using a polymer layer with a higher refractive index that is close or even higher than that of the NCF, which will increase the propagation losses as the polymer cover the NCF. We can also increase the resolution, as typically occurs in commercial sensors, by reducing the sensing range. This is achieved by reducing the thickness of the pressure membrane.

Regarding the cross-sensitivity with temperature, just as any other fiber sensor our pressure sensor is also sensitive to temperature. Temperature changes can modify the refractive index via thermo-optic effects and increment in size of the materials via the coefficient of thermal expansion (CTE). In the case of the MMI attached to the aluminum plate we can estimate the wavelength shift resulting from thermal effects [19]. We estimate a temperature sensitivity of 42 pm/°C which induces a wavelength shift of 2.4 nm at a maximum temperature of 80 °C. Based on the spectral response of our sensor (see Fig. 7) this induces a maximum intensity change of 0.0006 mW. Such variation could be neglected since it is smaller than the minimum intensity variation resolved by our sensor. In the case of the PDMS its refractive index value is reduced as the temperature is increased due to its negative thermo-optic coefficient (-4.5×10^{-4} °C^{-1}). This increases the refractive index difference between the No-Core fiber and the PDMS, which results in a better confinement of the modes in the contact area (as compared to lower temperatures) and should slightly reduce the propagation losses. On the other hand, the thermal expansion of the PDMS will increase the contact area as the temperature is increased, which results in higher propagation losses. Both thermal and expansion effects in the PDMS are opposite, and the net effect should be a change in the slope of the sensor response and a slight reduction on the sensing range. This can be compensated, as in the case of other fiber sensors, once we have characterized the temperature response of the sensor.

V. Conclusion

We have developed a pressure sensor using MMI effects. The principle of operation of the sensor is based on intensity changes of the MMI signal when the optical properties of the NCF are modified. This was achieved by pressing a PDMS polymer layer against a NCF. Since the PDMS is a soft material, its contact area around the circumference of the NCF increases as a function of applied pressure. The combination of PDMS around the NCF and stress induced in the NCF effectively reduce the number of propagating modes along the NCF, which reduces the transmitted MMI signal. Intensity changes are obtained by tracking a particular wavelength, achieving good linear response and repeatability with a sensitivity of -0.145×10^{-3} mW/kPa for pressure values up to 960 kPa. The sensor provides a simple and inexpensive design for a fiber based pressure sensor.

References

[1] B.-J. Peng, Y. Zhao, J. Yang, and M. Zhao, "Pressure sensor based on a free elastic cylinder and birefringence effect on an FBG with temperature-compensation," *Measurement*, vol. 38, no. 2, pp. 176–180, Sep. 2005.

[2] L. Mohanty, S. C. Tjin, and N. Q. Ngo, "Pressure mapping sensor with an array of chirped sampled fiber gratings," *Sens. Actuators A, Phys.*, vol. 117, no. 2, pp. 217–221, Jan. 2005.
[3] L. Liu, H. Zhang, Q. Zhao, Y. Liu, and F. Li, "Temperature-independent FBG pressure sensor with high sensitivity," *Opt. Fiber Technol.*, vol. 13, no. 1, pp. 78–80, Jan. 2007.
[4] W. J. Bock, J. Chen, P. Mikulic, and T. Eftimov, "A novel fiber-optic tapered long-period grating sensor for pressure monitoring," *IEEE Trans. Instrum. Meas.*, vol. 56, no. 4, pp. 1176–1180, Aug. 2007.
[5] M. Smietana, W. J. Bock, P. Mikulic, and J. Chen, "Tuned pressure sensitivity of dual resonant long-period gratings written in boron co-doped optical fiber," *J. Lightw. Technol.*, vol. 30, no. 8, pp. 1080–1084, Apr. 15, 2012.
[6] C. Wu, Y. Zhang, and B.-O. Guan, "Simultaneous measurement of temperature and hydrostatic pressure using Bragg gratings in standard and grapefruit microstructured fibers," *IEEE Sensors J.*, vol. 11, no. 2, pp. 489–492, Feb. 2011.
[7] D. Chen, G. Hu, M. L. V. Tse, and H. Y. Tam, "Design of a dual-core dual-hole fiber for hydrostatic pressure sensing," *Opt. Commun.*, vol. 285, nos. 10–11, pp. 2615–2619, May 2012.
[8] H. Y. Fu *et al.*, "Pressure sensor realized with polarization-maintaining photonic crystal fiber-based Sagnac interferometer," *Appl. Opt.*, vol. 47, no. 15, pp. 2835–2839, May 2008.
[9] D. Donlagic and E. Cibula, "All-fiber high-sensitivity pressure sensor with SiO_2 diaphragm," *Opt. Lett.*, vol. 30, no. 16, pp. 2071–2073, Aug. 2005.
[10] X. Feng *et al.*, "High-sensitivity Fabry–Perot interferometric pressure sensor based on a nanothick silver diaphragm," *Opt. Lett.*, vol. 37, no. 2, pp. 133–135, Jan. 2012.
[11] P. V. Rao, K. Srimannarayana, M. S. Shankar, P. Kishore, D. Sengupta, and P. S. Reddy, "Multimode fused coupler fiber optic pressure sensor," in *Proc. AIP Conf.*, vol. 1391, May 2011, pp. 450–452.
[12] N. K. Pandey and B. C. Yadav, "Embedded fibre optic microbend sensor for measurement of high pressure and crack detection," *Sens. Actuators A, Phys.*, vol. 128, no. 1, pp. 33–36, Mar. 2006.
[13] Q. Wang, G. Farrell, and W. Yan, "Investigation on single-mode–multimode–single-mode fiber structure," *J. Lightw. Technol.*, vol. 26, no. 5, pp. 512–519, May 1, 2008.
[14] J. E. Antonio-Lopez, A. Castillo-Guzman, D. A. May-Arrioja, R. Selvas-Aguilar, and P. LiKamWa, "Tunable multimode-interference bandpass fiber filter," *Opt. Lett.*, vol. 35, no. 3, pp. 324–326, Feb. 2010.
[15] F. Schneider, J. Draheim, R. Kamberger, and U. Wallrabe, "Process and material properties of polydimethylsiloxane (PDMS) for Optical MEMS," *Sens. Actuators A, Phys.*, vol. 151, no. 2, pp. 95–99, Apr. 2009.
[16] D. Armani, C. Liu, and N. Aluru, "Re-configurable fluid circuits by PDMS elastomer micromachining," in *Proc. 12th Int. Conf. MEMS*, Jan. 1999, pp. 222–227.
[17] V. V. Meleshko, "Bending of an elastic rectangular clamped plate: Exact versus 'engineering' solutions," *J. Elasticity*, vol. 48, no. 1, pp. 1–50, May 1997.
[18] W. S. Mohammed, A. Mehta, and E. G. Johnson, "Wavelength tunable fiber lens based on multimode interference," *J. Lightw. Technol.*, vol. 22, no. 2, pp. 469–477, Feb. 2004.
[19] E. Li, "Temperature compensation of multimode-interference-based fiber devices," *Opt. Lett.*, vol. 32, no. 14, pp. 2064–2066, Jul. 2007.

Daniel A. May-Arrioja received the B.Sc. degree in electrical engineering from the Instituto Tecnológico de Tuxtla Gutierrez, Mexico, the M.Sc. degree in optics from INAOE, Mexico, and the Ph.D. degree in optics from CREOL, College of Optics and Photonics, University of Central Florida, Orlando, USA. His current research interests include integrated photonics and fiber optics devices with applications to lasers, sensors and biosensors, and MEMS.

Victor I. Ruiz-Perez received the B.S. degree in mathematics and physics education from the University of Montemorelos, Montemorelos, Nuevo Leon, Mexico, and the M.Sc. and Ph.D. degrees in optics from the National Institute of Astrophysics, Optics and Electronics, Puebla, Mexico. His current research interests include the development of optical fiber sensors and biosensors.

Yaneth Bustos-Terrones received the B.Sc. degree in environmental engineering, the M.Sc. degree in sciences and environmental engineering, and the Ph.D. degree in sciences and environmental engineering from Autonomous Metropolitan University, México. Her current research is focused on wastewater treatment and the environment quality.

Miguel A. Basurto-Pensado received the Ph.D. degree in optics from the National Institute for Astrophysics, Optics and Electronics. He is currently a Full Professor with the Center for Research in Engineering and Applied Sciences, Universidad Autónoma del Estado de Morelos, Mexico. His research interests are fiber optics sensors and sensing technologies.